Available online at www.sciencedirect.com
ScienceDirect
International Journal of Heat and Mass Transfer 50 (2007) 226–239
International Journal of HEAT and MASS TRANSFER
www.elsevier.com/locate/ijhmt

Analysis of flow patterns emerging during evaporation in parallel microchannels

S. Hardt [a], B. Schilder [b], D. Tiemann [b], G. Kolb [b], V. Hessel [b], P. Stephan [a,*]

[a] Chair of Technical Thermodynamics, Darmstadt University of Technology, 64287 Darmstadt, Germany
[b] Institute of Microtechnology Mainz (IMM), 55129 Mainz, Germany

Received 19 December 2005; received in revised form 26 May 2006
Available online 10 October 2006

Abstract

The evaporation processes of 2-propanol and water in cyclo olefin polymer (COP) and silicon microchannels of square cross-section are studied with a high-speed camera. The COP channels with a cross-section of 50 μm × 50 μm are rather smooth, whereas the 30 μm × 30 μm silicon channels have comparatively rough surfaces. For the COP channels, two different evaporation modes are identified, both with oscillating liquid–vapor menisci. One of these modes is characterized by an extremely rapid evaporation and a corresponding discontinuous shift of the meniscus. In the silicon channels four different evaporation modes are observed. Oscillatory motion of the liquid fronts also dominates here, and depending on the total mass flow and the wall temperature the oscillations in different channels are synchronized or desynchronized. Besides the flow patterns also the velocity trajectories of the evaporating liquid fronts are analyzed in detail and show a rather good reproducibility over different channels and different cycles. Compared to most other studies reported in this field, bubble nucleation is found to be of secondary importance for the evaporation processes.

Keywords: Microchannels; Flow boiling; Flow patterns; Two-phase flow

1. Introduction

Flow boiling in microchannels and corresponding microchannel heat sinks or evaporators have been in the spotlight of many research activities in the past few years. A main driver for these activities is the exponentially increasing power dissipation of microelectronic circuits, which demands for high performance cooling systems [1]. In addition to that, microchannel evaporators find their applications in fields such as fuel processing technology for fuel cells, where high mass flow rates of gaseous fuel have to be produced by evaporation from a compact volume [2,3].

As discussed by Lasance and Simons [1], evaporation of water is among the mechanisms that promise the highest heat transfer coefficients for electronics cooling. When comparing single-phase liquid flows in microchannels with flow boiling, the latter usually requires less pumping power. In addition, the limit for the maximum achievable heat transfer coefficient is higher when allowing for phase change. These arguments underpin the considerable potential of two-phase microchannel heat sinks for dissipating the high heat fluxes emerging from state-of-the-art miocroelectronic devices. Owing to the ever-increasing integration density of electronic circuits, the demand for efficient cooling technologies is expected to increase substantially in the near future.

Fuel processing technology, a second application area for which flow boiling phenomena in microchannels have become relevant, poses similar demands on the heat transfer rates as electronics cooling technology. Corresponding micro evaporators are often designed for mobile fuel processing systems which means they should be compact and provide a vapor flow per unit volume as high as possible.

* Corresponding author. Tel.: +49 6151 163159; fax: +49 6151 166561.
E-mail address: pstephan@ttd.tu-darmstadt.de (P. Stephan).

0017-9310/$ - see front matter © 2006 Elsevier Ltd. All rights reserved.
doi:10.1016/j.ijheatmasstransfer.2006.06.015

Nomenclature

f	frequency [Hz]	R_a	average surface roughness [μm]
L	oscillation length [mm]	t	time [ms]
$\dot{m}$	mass flow per unit area [kg/(m^2 s)]	T_w	wall temperature [°C]

The heat fluxes transferred through such devices are usually comparable to those characteristic for electronics cooling applications [4]. The work presented in this article emerged from R&D activities on microchannel evaporators for fuel processing having been carried out at IMM over the past few years.

The flow regimes occurring during flow boiling in microchannels have been reviewed by a number of authors, among others by Kandlikar et al. [5,6] and by Thome [7]. Depending on the process conditions and especially on the channel shape and dimensions, different two-phase flow patterns may be found when evaporation of a liquid occurs in a small single channel or in a number of parallel channels. The evaporation mechanism most frequently observed starts with the creation of small bubbles at the walls of the microchannels. When the bubbles have reached a certain size they detach from the channel walls and are transported along with the flow. In comparatively small channels this may only occur when the bubbles have already reached the dimension of the channel diameter. Subsequently, the bubbles continue to grow, finally yielding elongated vapor slugs which are usually separated from the channel walls by a thin liquid film. Such vapor slugs may undergo coalescence or may merge with the advancing liquid–vapor meniscus. Corresponding nucleate boiling processes followed by film evaporation have been observed by a number of authors in microchannels of different shapes and sizes. Jiang et al. [8] have studied evaporation in triangular channels with hydraulic diameters of 40 and 80 μm. Hetsroni et al. [9–11] found the phenomenon in triangular channels with a width between 200 and 310 μm, while Serizawa et al. [12] have studied circular tubes with an inner diameter of 50 μm. The same scenario has been observed by Steinke and Kandlikar [13] in rectangular channels of 207 μm hydraulic diameter, by Lee and Mudawar [14] in rectangular channels with a cross-section of 713 μm × 231 μm, and by Li et al. [15] in trapezoidal channels of 48 μm hydraulic diameter. Koşar et al. [16–18] could show that the growth of bubbles against the flow direction in rectangular microchannels can be prevented by introducing flow restrictors to the inlet section. Similar results were obtained by Qu and Mudawar [19] and by Kandlikar et al. [20]. Liu et al. experimentally studied the conditions for onset of nucleate boiling in microchannels [21].

From all these studies it becomes apparent that bubbles are created even in microchannels of comparatively small diameter, a scenario that has been questioned in an earlier work of Peng et al. [22]. In this work the hypothesis has been formulated that bubble formation is suppressed in small channels and that there is a critical channel diameter defining a lower limit for nucleation of bubbles to occur. Comparing the different channel geometries which have been investigated there is a clear indication that bubble nucleation critically depends on geometric and topographic features of the channel walls. Bubble nucleation is usually initiated at specific nucleation sites which could be small cavities inside the channel walls due to irregularities or surface roughness or sharp corners in the cross-sectional area of a channel. The works of Xu et al. [23] and of Hetsroni et al. [11] provide a clear indication that in a triangular channel bubbles are formed preferably in the corners.

A further aspect of microchannel flow boiling which has been studied in some detail is the occurrence of periodic oscillations of the flow pattern and of related parameters such as the pressure drop in a channel. Wu and Cheng [24] performed a detailed analysis of the cyclic temperature, pressure and mass flow variations during evaporation in trapezoidal channels having a hydraulic diameter of 186 μm and determined oscillation periods between 15 and 202 s. Interestingly, Xu et al. [23] determined much smaller cycle periods in the range of 50 ms in their measurements for triangular channels with a hydraulic diameter of 155 μm. Cycle periods in the range between 20 and 150 ms were measured by Hetsroni et al. [11].

As mentioned before, evaporation in microchannels is usually initiated by bubble nucleation. In a few experiments, however, a rapidly receding liquid front was observed while no bubble formation could be detected. Such "eruptive boiling" phenomena were found by Zhang et al. [25], however, the time resolution of the CCD camera used was only about 33 ms. It seems that this boiling mode is characteristic for small channels (44 μm hydraulic diameter), since in the same series of experiments bubble nucleation was observed in channels of 171 μm hydraulic diameter. Hetsroni et al. [11] reported a similar scenario which they termed "explosive boiling". Working at a rate of 1000 frames per second they could similarly detect a rapidly receding liquid–vapor meniscus. However, they attributed this phenomenon to the nucleation of a bubble close to the advancing liquid front, followed by rapid growth and merging of this bubble with the vapor downstream of the meniscus. After all, the question whether or not there is a boiling mechanism in microchannels not being initiated by bubble nucleation seems to be not yet resolved.

Besides these experimental efforts to understand the flow boiling phenomena in microchannels there have been some attempts to gain a theoretical understanding of the processes involved. Park and Lee [26] studied the region

around an evaporating liquid–vapor meniscus and formulated a model for the thickness of the liquid layer from which the local heat transfer coefficient could be determined. Qu and Mudawar [27] studied heat transfer assuming an annular flow configuration, i.e. a situation where a vapor core is surrounded by a liquid film attached to the channel walls. Thome et al. [28] considered evaporating vapor slugs and subdivided the flow domain into three different regions, one containing solely liquid, the second with a liquid film of decreasing thickness and a third (dry) region containing only vapor. All of these models have in common that comparatively restrictive assumptions on the flow configuration are made. While the model results agree reasonably well with published experimental data [29], their applicability has clearly to be checked in each specific case. A more general approach towards boiling heat transfer in microchannels was pursued by Mukherjee and Kandlikar [30] who studied the growth of vapor bubbles based on the level-set method. Compared to the models described above, less assumptions have to be made but more extensive computational resources are required. In addition to these approaches allowing the computation of flow boiling heat transfer coefficients in microchannels, Li and Cheng [31] have developed a model for the onset of bubble nucleation in small-scale channels, taking into account effects from the velocity profile and from dissolved gases in the liquid.

In the present paper, flow boiling in parallel microchannels with quadratic or close-to-quadratic cross-sections of 30 μm × 30 μm and 50 μm × 50 μm is studied experimentally. Especially two aspects which have rarely been examined before are in the focus of the studies. First, an evaporation mode with a rapidly accelerating liquid front has been observed. For this convective boiling mechanism no bubble nucleation has been detected. Corresponding velocity curves and oscillation cycles are studied in detail. Secondly, the collective behavior of the system comprising a number of parallel microchannels is analyzed, where the term "collective" refers to the correlation between the flow patterns in different channels. As will be discussed in the following sections, synchronized or desynchronized behavior of parallel channels is found depending on evaporation mass flux. Besides its importance for the fundamental understanding of microfluidic multichannel systems, the latter aspect should also bear some practical importance, since microchannel heat sinks or evaporators usually comprise a number of parallel channels.

2. Experimental

2.1. Microchannel fabrication

Two different types of microchannel devices were used for studying flow boiling phenomena. The first device was fabricated by hot embossing from a cyclo olefin polymer (COP, Zeonor 1420 R, Zeon Europe GmbH, Düsseldorf, Germany) substrate. The master structure for the embossing process was obtained via Deep Reactive Ion Etching (DRIE) in silicon allowing creation of almost vertical side walls. Subsequently, the voids formed in the silicon wafer were filled with nickel in an electroforming step and the silicon was removed by wet etching. The master structure obtained in that way was used for embossing a COP chip with outer dimensions of 85 mm × 55 mm × 2 mm, resulting in 300 parallel channels with a cross-section of approximately 50 μm × 50 μm and a length of 64.5 mm. Upstream of the channel inlets there is a flow distribution region with a dimension of 46 mm × 6 mm × 1.8 mm, a similar fluidic chamber connects the channels downstream of their outlets. The top of Fig. 1 shows a REM image of corresponding channel structures, giving an indication of the comparatively smooth surfaces and vertical walls with an average roughness of $R_a = 0.5$ μm. In a final step the COP chip was sealed by a COP sheet with a thickness of 90 μm using a solvent bonding method. On the bottom of Fig. 1 the complete chip is displayed. Further details of the fabrication process can be found in [32].

As described above, the DRIE process in combination with hot embossing results in comparatively smooth channel walls. It is well known that small cavities in a solid surface may act as nucleation sites for boiling. For this reason a second microchannel device with a higher surface roughness was fabricated, thus possibly providing a larger number of nucleation sites. Laser ablation of silicon enables fabrication of small channels with a high roughness value.

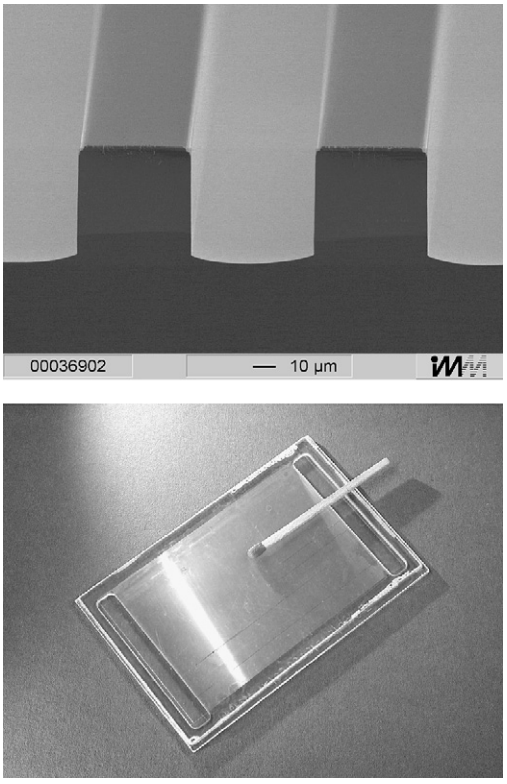

Fig. 1. REM image of the microchannel structures of the COP chip (top), and total view of the chip showing the inlet and outlet chambers (bottom).

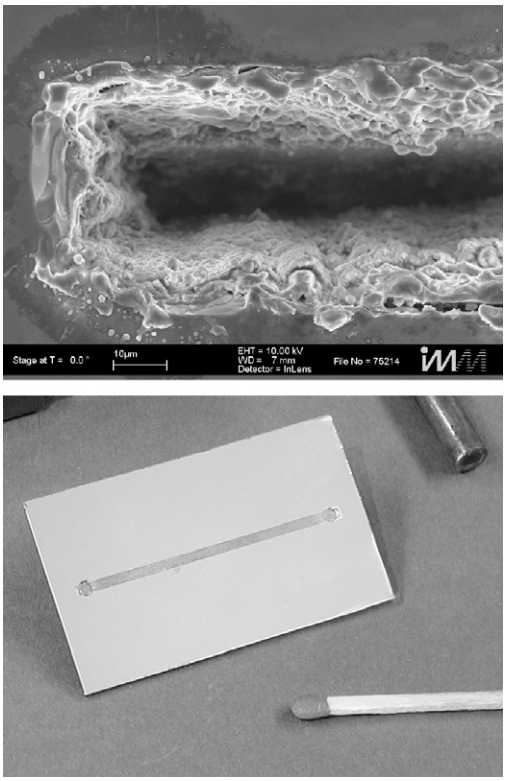

Fig. 2. REM image of a channel obtained by laser ablation of silicon (top), and total view of the silicon chip containing 16 parallel channels (bottom).

In a 600 μm thick silicon wafer 16 parallel channels with a cross-section of approximately 30 μm × 30 μm and a length of 43.5 mm were created using a frequency-doubled Nd:YAG laser with a wavelength of 532 nm (Scanlab AG, Puchheim, Germany). This process yields comparatively rough channel surfaces ($R_a = 4$ μm), as displayed on the top of Fig. 2. After laser ablation the debris deposited on the surface of the silicon wafer was removed by polishing the wafer for 45 min with a diamond polishing disk (grain size 1 μm). Subsequently, the channels were sealed with a Pyrex cover of 600 μm thickness (Corning GmbH, Wiesbaden, Germany) via anodic bonding for 45 min at a temperature of 410 °C and a voltage of 600 V. The resulting device with 16 parallel channels between inlet and outlet holes of 1.6 mm diameter is shown on the bottom of Fig. 2.

2.2. Experimental setup and methods

Slightly different experimental setups were used to study the performance of the two microchannel evaporators. Fig. 3 shows the setup used for the COP evaporator. The COP chip is pressed onto an aluminum plate of 2 mm thickness below which a Vermiculite insulation layer of 20 mm thickness is arranged. Between the insulation layer and the aluminum plate is a heating mat (Watlow GmbH, Kronau, Germany) and a thermocouple (Reckmann GmbH, Hagen, Germany) with 0.5 mm diameter enabling temperature measurements. The signal of the thermocouple provides the

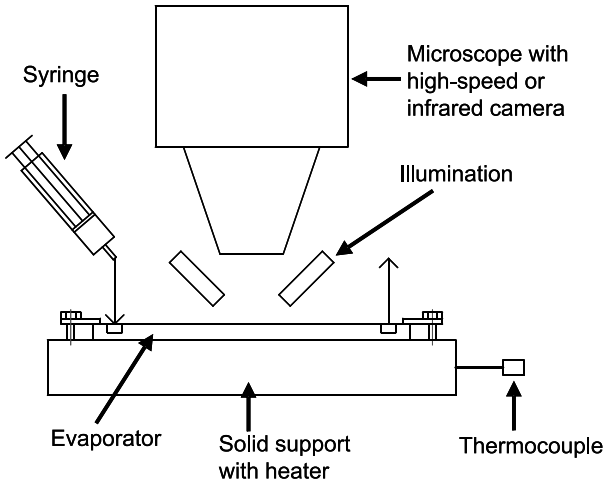

Fig. 3. Schematic of the experimental setup for the COP evaporator.

input for a thermal control unit (Evolution Technologies, Mainz, Germany) allowing to fix the temperature to a predefined value. Liquid is delivered to the flow distribution chamber of the COP chip by a syringe. In this case the syringe merely acts as a liquid reservoir and not as a pump, as the liquid transport through the microchannels is solely achieved by capillary forces. The two-phase flow patterns inside the channels are detected by a CMOS high-speed camera with a frame rate of up to 20,000 fps (Basler A 504 kc, Basler Vision Components, Exton, PA) mounted on a microscope (Zeiss Stemi SV 11, Carl Zeiss AG, Oberkochen, Germany). For illumination up to four fiber-optic cold light sources (Schott KL 1500, Schott AG, Mainz, Germany) were used. The temperature distribution on the chip surface can be measured by an infrared camera (FLIR ThermaCAM SC500, FLIR Systems, Wilsonville, OR) which replaces the microscope in this case.

The setup for the silicon evaporator is based on the same idea but is slightly modified, as displayed in Fig. 4. The chip is pressed onto a stainless steel block with dimensions of 54 mm × 52 mm × 20 mm which contains two boreholes for heating cartridges (Watlow Firerod, Watlow GmbH, Kronau, Germany). Temperature control is performed in the same way as described above based on a thermocouple measuring the temperature inside the steel block. For the fluid supply to the chip a syringe pump (KD Scientific 230, KD Scientific Inc., Holliston, MA) is used. The fluidic connection is provided via a clamping frame. For this reason the chip does not completely rest on the steel block, but there is an unsupported area extending for 15 mm between the fluidic inlet and the edge of the block. The same illumination, microscope and high-speed camera are used as above. In contrast to the COP chip, the temperature of the solid substrate is now measured by a thermocouple attached to the outlet hole of the chip and in contact with the silicon substrate.

For both devices the temperature was kept fixed using the described control unit. Owing to the small thickness of the silicon wafer (600 μm) and the high thermal conductivity of silicon, only very small out-of plane temperature

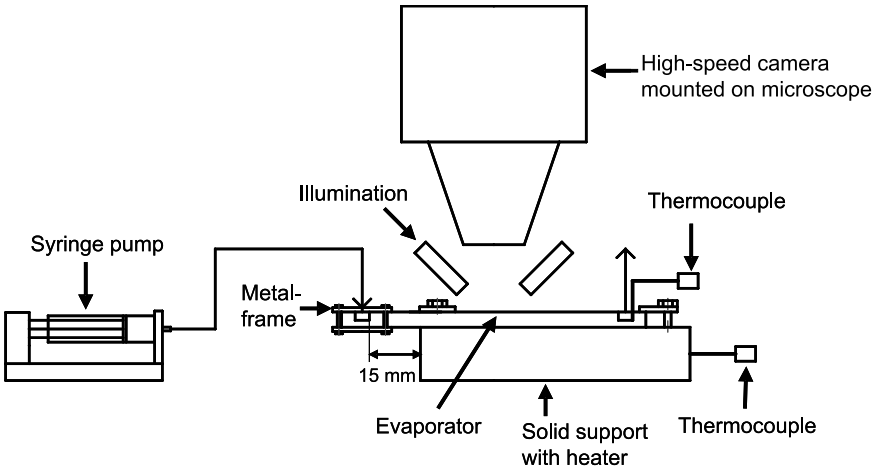

Fig. 4. Schematic of the experimental setup for the silicon evaporator.

gradients are expected in this case. As a result of the small thermal conductivity of polymers, this no longer needs to be true for the COP evaporator. However, the outlet chamber of the COP chip visible in Fig. 1 is open to the environment (i.e. only one side is covered by a polymer sheet) and by IR thermography the temperature can directly be measured at the thin COP sheet covering the channels which is exactly the position of interest in the out-of-plane direction. The in-plane temperature gradients are expected to be small in both cases because both chips are in contact with highly conductive metal surfaces, with the exception of the inlet region of the silicon chip. Experimental support for this statement is provided by the IR images taken from the chip surface, to be discussed below.

A limiting factor for the flow-pattern visualization with the high-speed camera is the amount of light available for one frame. On the one hand, the amount of light collected is reduced by using a microscope and limiting the visible area of the chip surface to about 2 mm × 2 mm, as was done for the experiments described here. One the other hand, the brightness of the images is further reduced by increasing the shutter speed of the camera. With these constraints a maximum frame rate of 5000 fps could be reached when using four independent light sources with illumination units in a cone-like arrangement about 5 mm away from the area of interest.

As already indicated, an evaporation mode to be analyzed in this article is characterized by a rapidly accelerating liquid–vapor meniscus (also termed "liquid front"). In order to determine the velocity of the meniscus as a function of time, a scale was projected onto the digitized images and the position of the meniscus was determined via an eyeball fit. The calibration of the scale was done by comparing with the spatial period of the repetitive channel structures. While the width of a single channel can deviate from its target value due to inaccuracies in the microfabrication process, the spatial period of the structures is defined with high accuracy. Velocities were then simply determined by dividing the difference in position by the time difference.

2.3. Materials

Deionized, filtered water and 2-propanol with a purity of more than 99% (Fluka, Buchs, Switzerland) were used as working liquids. According to [33], the saturation temperature and enthalpy of vaporization of these two liquids at standard pressure are given as 100.0 °C, 40.66 kJ/mol (water) and 82.3 °C, 39.85 kJ/mol (2-propanol). Owing to the large surface-to-volume ratio in microchannels, wetting forces are expected to play a predominant role. For this reason the contact angle for the four different liquid/solid combinations was measured using a goniometer (Krüss G1, Krüss Optronic GmbH, Hamburg Germany). Three independent measurements were performed for each combination, the corresponding results are listed in Table 1. It is worth while to note that 2-propanol has a very small contact angle of less than 10° on both surfaces.

2.4. Uncertainty analysis

When determining the velocity of the liquid–vapor menisci by analyzing the images taken with the high-speed camera, the uncertainty is mainly due to possible errors in localizing the liquid front. From the image analysis procedure the uncertainty is estimated to be of the order of 10^{-2} m/s, translating to ±2% for a velocity of 0.5 m/s and ±10% for 0.1 m/s. Concerning the oscillation period of the evaporation process, a cycle was typically resolved with 200 frames. Assuming that the start or the end of a period can be detected with an accuracy of ±2 frames, its duration can be determined with an accuracy of ±1%. In

Table 1
Measured contact angles for the different material combinations

Material combination	Average value [°]	Standard deviation [°]
Water/COP	89	1.2
Water/silicon	20	4.6
2-Propanol/COP	6	2.0
2-Propanol/silicon	9	0.6

the silicon evaporator the total volume flow in the channels is determined by the flow rate of the syringe pump. According to the specification of the supplier, the uncertainty of the flow rate is ±1%.

Concerning the temperature measurements, the supplier value for the accuracy of the thermocouples used in the silicon evaporator is ±1.5 K. For the COP evaporator the solid temperature was determined using the IR camera which is not possible in a straightforward manner in the former case because of the partial IR transparency of silicon. Calibration of the camera was done using a thermocouple which was introduced into a small hole which had been drilled into the COP substrate at the location of the outlet chamber. Again, the maximum deviations of the temperature measurement with the thermocouple fall in a range of ±1.5 K. The IR camera itself provides a thermal resolution of ±0.08 K for a base temperature of 30 °C.

Since a point in the outlet chamber was chosen as reference point for determining the temperature of the COP substrate, an additional uncertainty may arise from in-plane (i.e. lateral) temperature variations in the chip. Such variations may arise if the thermal contact of the chip to the aluminum plate is imperfect, a situation which could be caused by deviations of the polymer substrate from planarity. For this reason the temperature distribution over the chip surface was recorded over the domain of the 300 parallel microchannels using infrared thermography. The measurement should provide an upper limit for the expected temperature deviations between different channels which is found to be about ±1 K.

3. Results and discussion

3.1. Flow patterns and flow maps

3.1.1. Flow patterns in the COP evaporator

Owing to the fact that infrared radiation has a very short absorption length in polymeric materials, the temperature of the chip surface can be determined via IR thermography. The temperature distribution recorded with the IR camera shows a good uniformity over the microchannel domain and seems to be independent of the liquid flow inside the channels. A point at the outlet of the channels has been chosen as reference point for the temperature measurements.

Owing to problems with thermal stresses, the measurements with the COP evaporator were only performed with 2-propanol as working liquid. At temperatures required for evaporation of water, thermal stresses induce cracks in the polymer material and destroy the test device. Two types of evaporation processes have been observed in the temperature range between 82 °C (saturation temperature of 2-propanol) and 93 °C. Both of them are periodic and involve evaporation of a thin liquid film. The first one is a film evaporation process with a continuous acceleration of the meniscus, in the second one film evaporation is preceded by eruptive evaporation.

3.1.1.1. Film evaporation with continuous acceleration of the meniscus. This cyclic evaporation process takes place inside the microchannels without any bubble nucleation. Fig. 5 sketches one cycle of this process, consisting of (1) capillary filling of the channel; (2) sudden acceleration of the liquid front in the opposite direction, leaving behind a film on the channel walls and a bubble at the channel entrance; (3) evaporation of the liquid film.

Corresponding photographic images are displayed in Fig. 6, where the drawing on the top of the figure indicates in which section of the channel the pictures were taken. The measurements were performed at a solid temperature of 86 °C with a resolution of 1000 fps and show the following scenario:

A1, $t = 0$ ms: liquid fills the channel driven by capillary forces;
A1, $t = 14$ ms: capillary filling stops;
A1, $t = 18$ ms: the curvature of the meniscus increases and the meniscus starts to accelerate in the opposite direction (to the left);
A2, $t = 24$ ms: an evaporating liquid film remains at the channel wall;
A2, $t = 424$ ms: the film is evaporated;
A1, $t = 945$ ms: the channel is refilled and the next cycle starts.

3.1.1.2. Film evaporation with preceding eruption. The progress of film evaporation with preceding eruption is similar to the evaporation process described above. However, here a very rapid ("discontinuous") shift of the liquid front is observed when its motion is reversed. Such an eruptive evaporation only takes place in channels which display

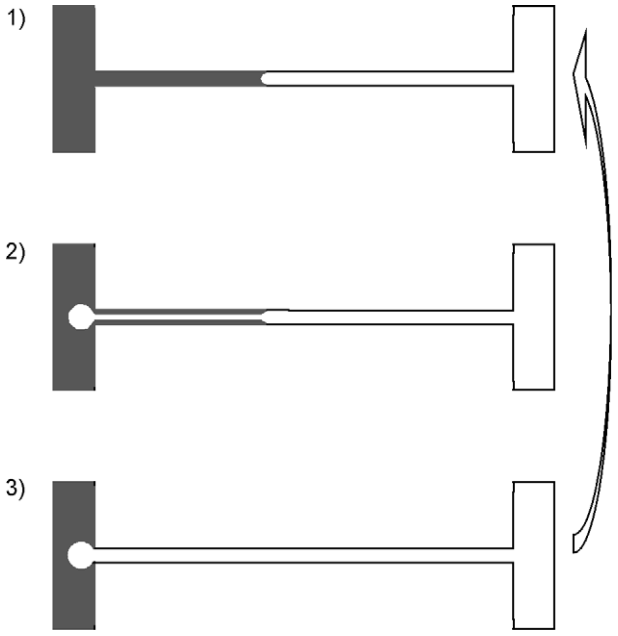

Fig. 5. Sequence of film evaporation with continuous acceleration of the meniscus.

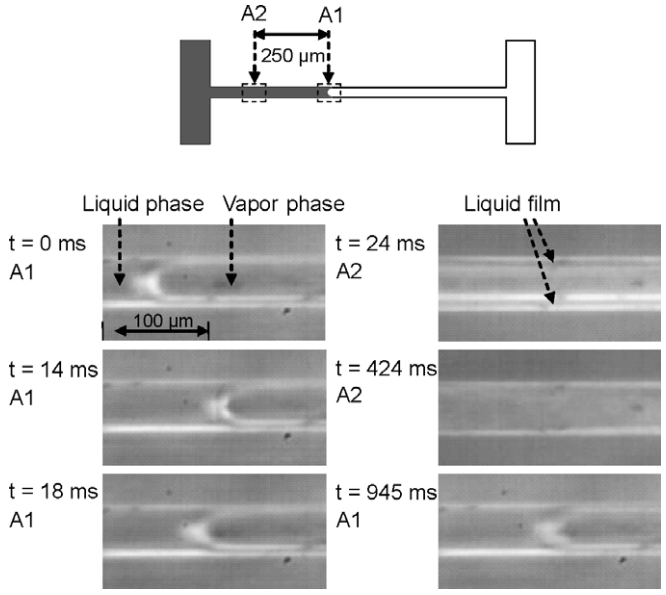

Fig. 6. Film evaporation with continuous acceleration of the meniscus, $T_w = 86$ °C, frame rate: 1000 fps.

some localized imperfections at their walls. Two different classes of imperfections ("cavities") have been observed, one with a characteristic size between 2 and 3 μm, the other measuring between 10 and 15 μm. Besides total draining of the channel over one cycle as described above, also partial draining was observed. This process only occurred when large cavities were present and for wall temperatures between the saturation temperature of 2-propanol (82.3 °C) and 90 °C. When only evaluating a single channel the wall temperature range for partial draining is about 3 K. The exact values of the upper and lower limit of this interval differ from channel to channel. Below the lower limit no evaporation process could be observed, above the upper limit total draining occurs. Fig. 7 depicts the evaporation process with preceding eruption. In the version with total draining (version a), the sequence is

(1) capillary filling of the channel;
(2) retraction of the meniscus, creation of a bubble at the channel entrance. The meniscus recedes explosively until it reaches the imperfection, after that its speed is slower and almost constant. An evaporating film remains at the channel wall;
(3) completion of film evaporation.

The difference of version b, the case with partial draining, is that the meniscus does not recede completely from the channel, but reverses its motion at a short distance behind the imperfection.

In order to resolve this process as good as possible, the frame rate of the high-speed camera was set to 5000 fps. A corresponding sequence of images taken for a solid temperature of 90 °C is shown in Fig. 8 and described as

$t = 0$ ms: liquid fills the channel driven by capillary forces;
$t = 17.2$ ms: the filling stops. The meniscus starts to vibrate;
$t = 17.4$ ms: the liquid portion between the imperfection and the meniscus evaporates eruptively;
$t = 17.6$ ms: the meniscus has reached the cavity. A liquid film covers the channel wall which is also visible in regions where previously no liquid has been;
$t = 48.4$ ms: the meniscus keeps moving to the left and the liquid film evaporates;
$t = 184.4$ ms: the channel is refilled and the procedure starts again.

3.1.2. Flow patterns in the silicon evaporator

For the silicon evaporator problems of material failure did not occur and 2-propanol was replaced with water which has a higher saturation temperature. The total mass flow rate was fixed by setting a specific value at the syringe pump which drives the liquid. Fixing the mass flow rate

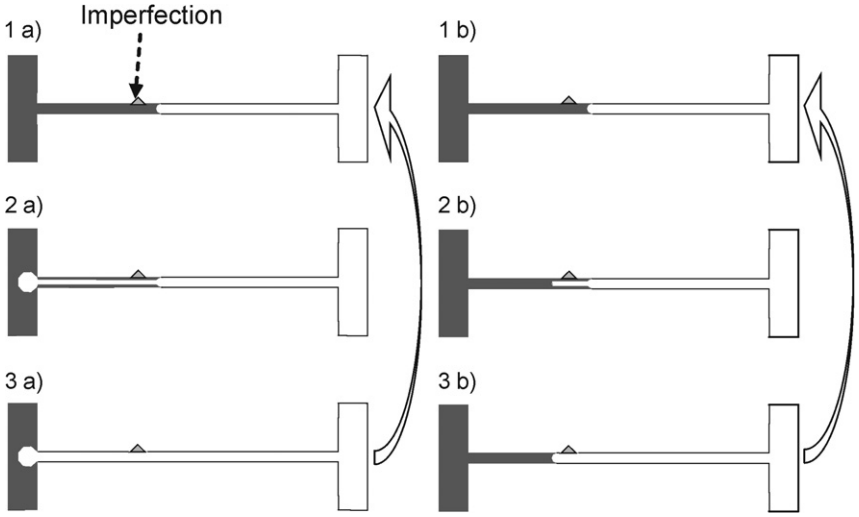

Fig. 7. Sequence of film evaporation with preceding eruption.

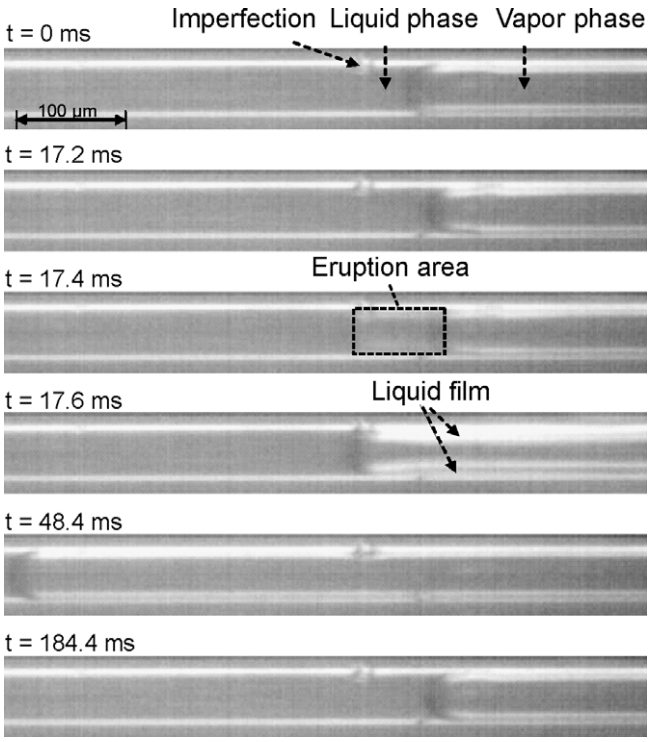

Fig. 8. Film evaporation with preceding eruption, $T_w = 90$ °C, frame rate: 5000 fps.

within reasonable limits has not been not possible with the COP evaporator, since from a certain mass flow rate on cross talk between neighboring channels due to imperfect sealing between the substrate and the cover sheet was observed. In contrast, the silicon evaporator allows variation of the total mass flow in a broad range. Besides the flow rate, the wall temperature is a second parameter determining the flow patterns emerging inside the channels. It turned out that varying these two control parameters changed the collective character of the evaporation mode. Two distinct modes observed in this context were synchronized and de-synchronized oscillations in the parallel channels. Paying regard to the collective behavior of the flow in the multichannel domain, four different evaporation modes could be identified, to be described in the following.

Stationary menisci: The menisci remain at a fixed position in spite of a constant, nonzero liquid flow (Fig. 9).

Parallel oscillations: Periodic retraction and refilling of liquid occur over a channel length of about 7 mm. All of the menisci oscillate with the same frequency and in phase (Fig. 10).

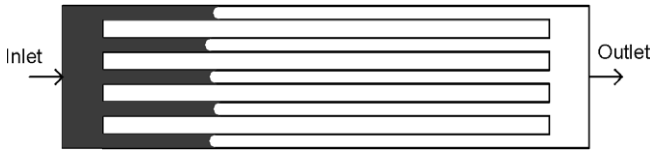

Fig. 9. Evaporation process with stationary menisci.

Chaotic oscillations: The oscillations are more irregular, the two extreme points of the periodic motion vary from channel to channel (Fig. 11). Also the frequencies vary and a phase correlation does no longer exist. Isolated bubbles are created within the channels, move with the liquid, grow and finally penetrate the liquid fronts.

Nucleate boiling: The liquid menisci no longer perform an oscillatory motion. Bubble formation is much more frequent compared to the chaotic oscillation regime (Fig. 12).

A photographic image of a characteristic fluid distribution in the silicon microchannels is shown in Fig. 13. In the upper channel a liquid film is attached to the walls, whereas the lower channels are dry. Such a film may either be left behind from a receding meniscus or it may separate a vapor slug from the solid surface.

The flow patterns in the silicon evaporator were recorded for a number of different points in the $(\dot{m}, T_w)$ plane, where the wall temperature was measured by the thermocouple in the outlet section of the evaporator, as described in the experimental section. From this parameter study a flow regime map was created which is shown in Fig. 14. Each of the crosses corresponds to one point in the $(\dot{m}, T_w)$ plane for which the flow pattern was evaluated.

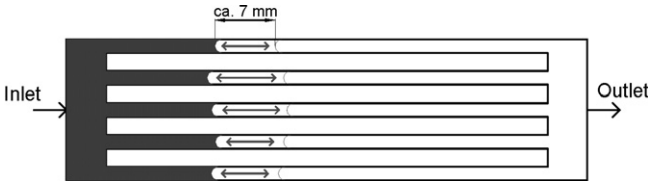

Fig. 10. Parallel oscillations of the menisci.

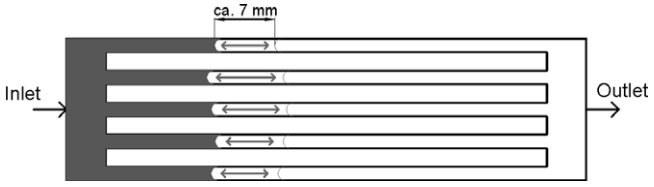

Fig. 11. Chaotic oscillations of the menisci.

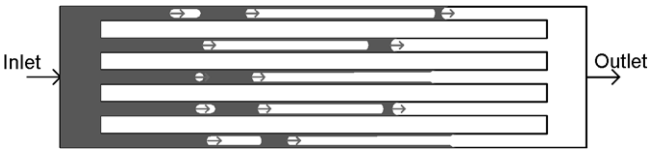

Fig. 12. Flow pattern in the nucleate boiling regime.

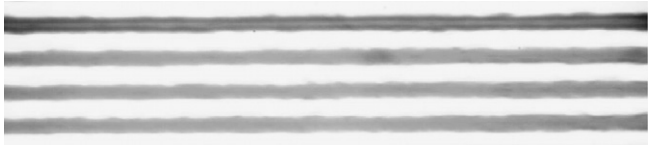

Fig. 13. Photographic image showing a section of four parallel channels with a liquid film attached to the uppermost channel.

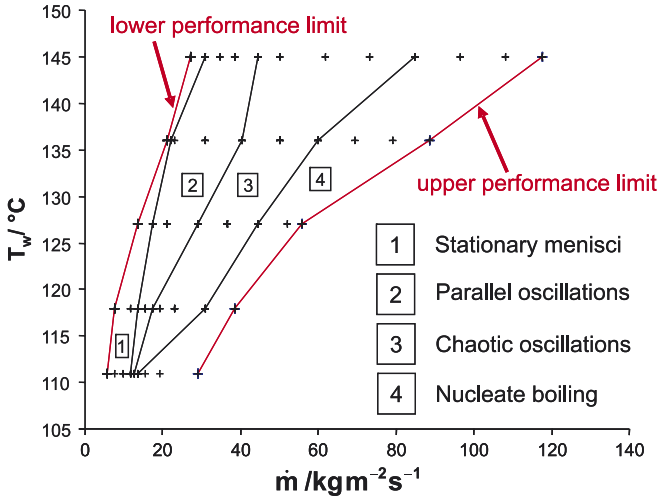

Fig. 14. Flow regime map for the silicon evaporator. The solid lines delineate different flow regimes.

The operation range of the evaporator is confined by the upper and lower limit of performance. Operating the evaporator to the left of the lower limit resulted in inhibition of the liquid supply for which vapor bubble formation in the inlet section is supposed to be the reason. Above the upper limit of performance liquid droplets could be observed in the vapor stream at the evaporator outlet. Hence this limit marks the transition from an outlet vapor quality of 1 to lower levels.

3.2. Velocity trajectories of the meniscus

The term "velocity trajectory" refers to the temporal evolution of the velocity of the liquid fronts during evaporation in microchannels. Such an analysis hardly seems to have been performed before. Xu et al. [23] reported some basic data on the liquid front velocity as a function of time. In the present work a more detailed and extended analysis of velocity trajectories is carried out. The purpose of such an analysis is to provide a database for a better understanding of microscale phase change phenomena and also to make available benchmark data for mathematical models of microchannel evaporation.

3.2.1. Velocity trajectories in the COP evaporator

The very nature of the two different flow patterns found in the COP evaporator translates to two different types of velocity trajectories.

3.2.1.1. Film evaporation with continuous acceleration of the meniscus. When the motion of a meniscus is reversed, it is continuously accelerated. Fig. 15 displays the velocity trajectories of nine evaporation cycles (three different channels, three cycles per channel). Note that the velocity values are negative because the transport is opposite to main flow direction. The origin of the time axis was chosen such that for the first measured data point of each curve the absolute value of the velocity is bigger than 0.03 m/s.

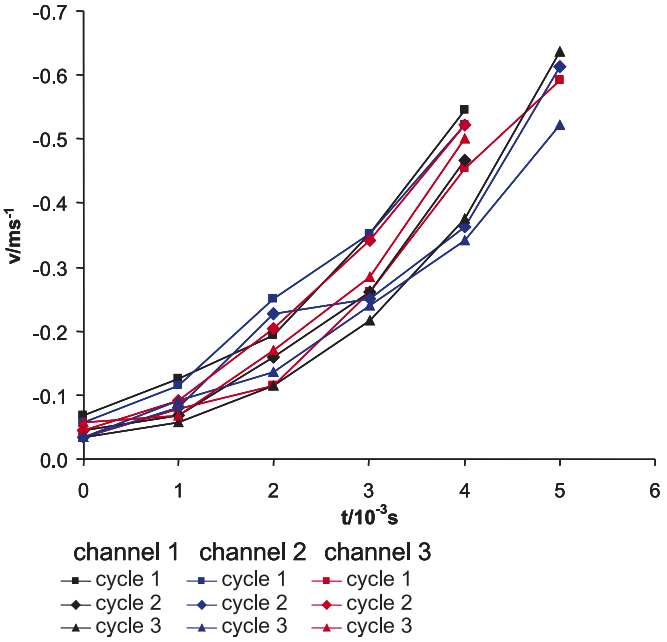

Fig. 15. Velocity trajectories in the COP evaporator for $T_w = 93$ °C.

Apparently, the different curves agree quite well, i.e. the acceleration phase of the motion is reproducible over different channels and different cycles. Inspections over the whole channel length have shown that the velocity levels off at values between 0.5 and 1.3 m/s.

3.2.1.2. Film evaporation with preceding eruption. This process starts with an explosive acceleration until the liquid front reaches the imperfection at the wall. The following channel draining process proceeds with a roughly constant speed of approximate 0.5 m/s, i.e. no further acceleration could be measured after the eruptive evaporation. Fig. 16 shows the velocity trajectories of three evaporation cycles, where the time origin was chosen to coincide with the point where reverse motion of the meniscus starts. Apparently, the velocity trajectories are highly reproducible.

3.2.2. Velocity trajectories in the silicon evaporator

Of the three different nontrivial flow patterns described above (the pattern with stationary menisci is considered as trivial) only the pattern with parallel oscillation of the liquid fronts possesses enough regularity and reproducibility to enable a reasonable analysis of velocity trajectories. A point making this analysis more difficult was the occasional formation of bubbles inside the channels. When a bubble is created it moves with the flow towards the meniscus, penetrates it and finally merges with the vapor phase. In the velocity trajectories such an event is visible as a sudden reduction of the velocity (as before, velocities in the direction of mass flow are counted as positive). For the data to be presented in the following, only one bubble formation events did occur.

The velocity trajectories for parallel oscillation are presented in Figs. 17–19 for different wall temperatures and

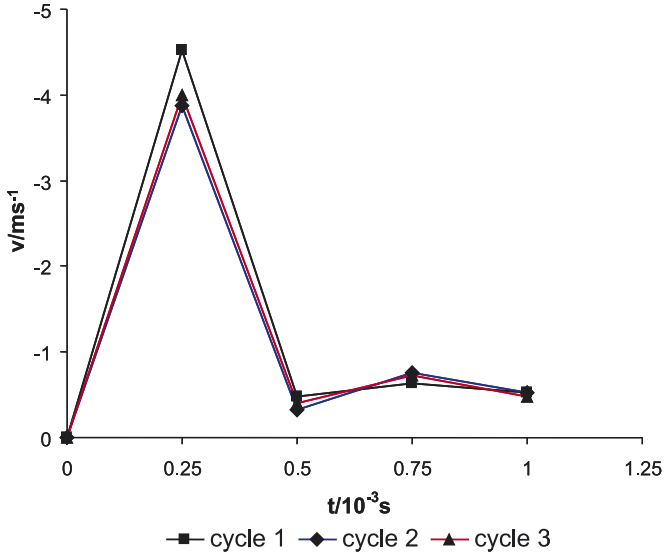

Fig. 16. Explosive acceleration of the liquid front in the COP evaporator for $T_w = 93$ °C.

total mass flows. Every diagram displays three successive cycles in five neighboring channels. Each top of the figure displays the individual trajectories, each bottom the average of the five individual curves. Note that the average was computed including the "bubble events", i.e. no attempt was made to eliminate the influence of bubbles

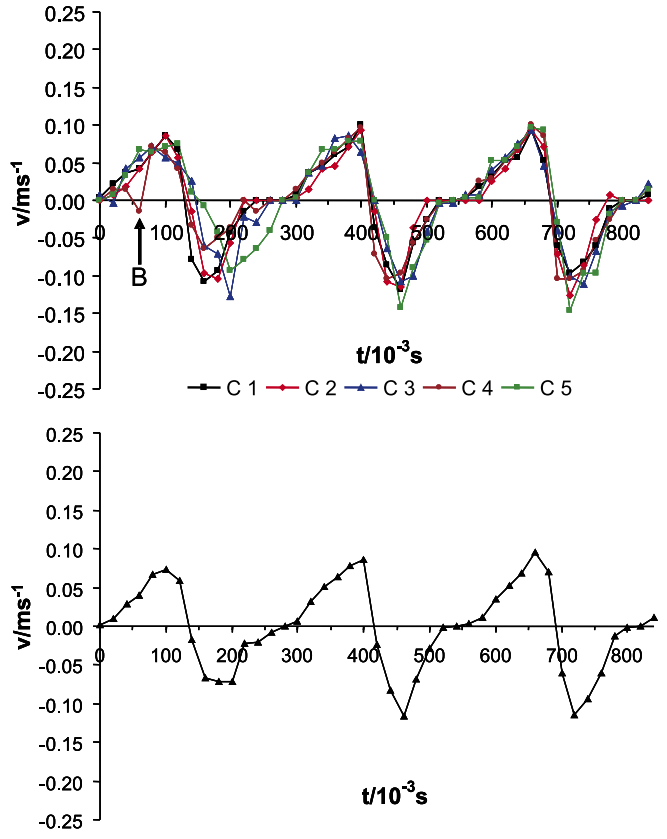

Fig. 17. Velocity trajectories at $T_w = 127$ °C, $\dot{m} = 21.2$ kg/(m^2 s). A bubble formation event is marked with a "B".

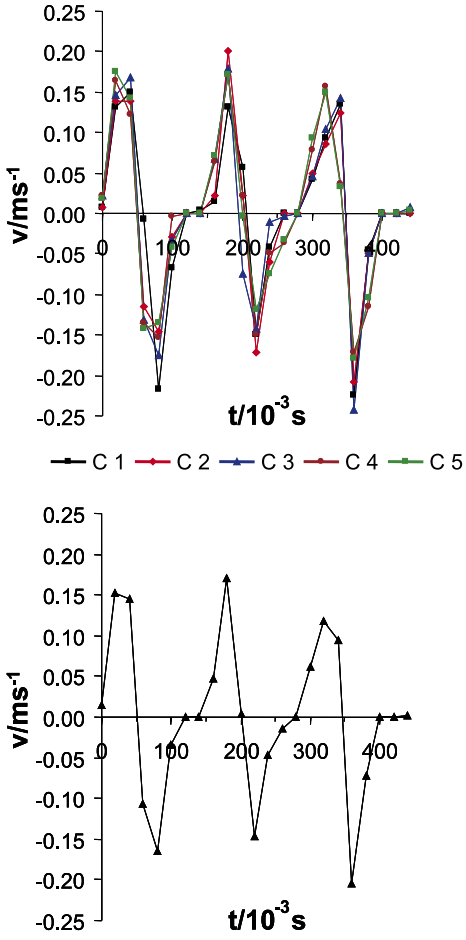

Fig. 18. Velocity trajectories at $T_w = 145$ °C, $\dot{m} = 34.7$ kg/(m^2 s).

on the velocity trajectories. Apart from events where a meniscus is penetrated by a bubble, the reproducibility of the velocity trajectories is rather good. The intersection of the curves with the x-axis represents the two turning points of the cycles, one marking the transition from forward to backward motion, the other the transition to refilling of the channel. A characteristic feature of the velocity trajectories is their asymmetric sawtooth shape. At the turning point marking the transition to refilling of the channel, the acceleration is very small. In contrast, the absolute value of the acceleration is large at the transition from forward to backward motion. The correlation between the channels is very pronounced, the oscillations are almost perfectly in phase. A comparison of Figs. 18 and 19 reveals that an increase in mass flow leads to a desynchronization of different channels, as already indicated by Fig. 14 which shows that increasing mass flow means approaching the regime of chaotic oscillations.

From the periodic trajectories the oscillation frequencies can be determined. In addition to that, the oscillation length which is the distance between the two turning points has been measured. The results of this analysis together with the corresponding standard deviations are listed in Table 2, where two more data sets with intermediate temperatures and mass flows have been analyzed. When

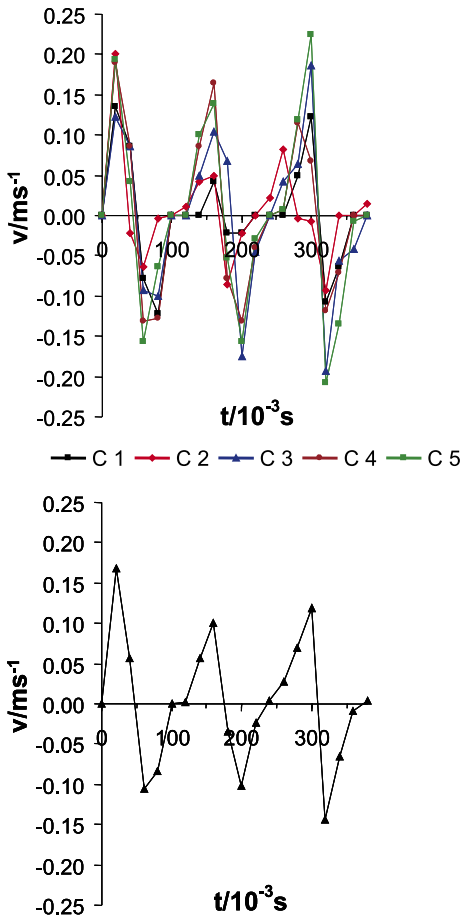

Fig. 19. Velocity trajectories at $T_w = 145$ °C, $\dot{m} = 38.6$ kg/(m^2 s).

Table 2
Oscillation frequency f and oscillation length L together with their standard deviations for different wall temperatures and mass flow rates

T_w [°C]	$\dot{m}$ [kg/(m^2 s)]	f [Hz]	Δf [Hz]	L [mm]	ΔL [mm]
127	21.2	3.45	0.42	7.0	0.7
136	23.1	5.21	0.12	7.2	1.3
136	30.9	5.45	0.33	7.3	0.4
145	34.7	7.06	0.43	6.3	0.5
145	38.6	7.45	0.46	5.5	1.2

trying to determine the influence of the wall temperature and the total mass flow on the oscillation frequency and length, one has to bear in mind that these two parameters cannot be varied independently, as otherwise one would leave the parallel oscillation regime (cf. Fig. 14). From the available data it seems that both an increase of the wall temperature and of the mass flow leads to a higher oscillation frequency. A trend for the dependency of the oscillation length on these two parameters did not become apparent.

3.3. Discussion

3.3.1. COP evaporator

Two different evaporating processes have been observed in the COP evaporator, film evaporation with continuous acceleration of the meniscus and film evaporation with preceding eruption. Most other authors observed an evaporation process which is initiated by bubble nucleation, which, however, is largely absent in the results reported here. Apart from a few imperfections in the channel walls, the COP surfaces fabricated by hot embossing are quite smooth. In addition, the contact angle for 2-propanol on COP is only 6 degrees. It is well known that for low-contact angle liquids the formation of nucleation embryos is largely suppressed [34]. In combination with a low surface roughness this could explain the absence of nucleate boiling in the parameter range studied here.

It suggests itself that the observed evaporation with preceding eruption represents an exception. In Fig. 8 an imperfection at the channel wall close to the liquid–vapor meniscus is clearly visible. As evaporation with preceding eruption was only observed in the vicinity of such imperfections it is natural to assume that a cavity in the wall surface initiates bubble nucleation. Subsequently, the bubble penetrates the liquid–vapor meniscus and gives the impression of an eruptive evaporation of the liquid volume between the imperfection and the meniscus. Bearing in mind that the process of bubble formation and growth could not be resolved even at a frame rate of 5000 fps, it is clear that the corresponding dynamics must be extremely fast. In their studies of microchannel boiling Hetsroni et al. [11] found a rapid evaporation process which they termed "explosive boiling". This process was attributed to the formation of a bubble closely behind the liquid–vapor meniscus. However, in their experiments the time scale for bubble formation and growth was determined to be about 10 ms which is much longer than the time scales reported here. Eruptive evaporation was also observed by Zhang et al. [25], however, with a rather poor time resolution of only 30 fps. Also Zhang et al. attribute the rapid evaporation process they have found to heterogeneous nucleation at the channel walls.

The other evaporation mode observed in the COP evaporator, film evaporation with continuous acceleration of the meniscus, is independent of any visible imperfections in the channel walls. For this reason it suggests itself to assume that there is no bubble nucleation involved. To the current point, only hypothetical explanations may by given on what causes the observed dynamics with a continuously accelerating meniscus leaving behind a thin liquid film on the channel walls. Owing to the small contact angle between 2-propanol and COP, wetting forces play a major role, thus favoring the film formation. As soon as evaporation starts, a vapor flow towards the outlet is created which has a much higher velocity than the liquid flow because of the density difference of about three orders of magnitude. This vapor flow causes a viscous pressure drop and a corresponding pressure force on the liquid–vapor meniscus. Apart from the very fact that the shape of the liquid front simply changes due to evaporation, this overpressure could be a part of the reason for the deformation and retraction of the meniscus. Compared to liquid/vapor interface

dynamics at room temperature, a deformation of the interface is facilitated for an evaporating meniscus since interfacial tension decreases as a function of temperature. The creation of a liquid film at the channel walls is expected to be related to the accelerated motion of the liquid front. When the meniscus recedes, the length of the film increases. Assuming that the phase change mainly occurs by film evaporation, the evaporation rate increases as the meniscus withdraws, yielding a pressure drop in the vapor phase increasing with time. As a result, the pressure force on the liquid/vapor interface rises and may possibly induce an accelerated motion. This accelerated motion levels off at front propagation speeds between 0.5 and 1.3 m/s where apparently a cancellation of the acceleration due to evaporation and forces on the meniscus has been reached.

Correlations between the flow patterns in the channels of the COP evaporator could not be observed in a similar manner as for the silicon evaporator. In the evaporation mode with continuous acceleration of the meniscus, all other channels were active as well and similar flow patterns were found. However, no simple correlation between the dynamics in different channels became apparent. Mainly this is due to the different oscillation length in different channels which results in different oscillation frequencies and phases. Nevertheless, the velocity trajectories in different channels are similar, as apparent from Fig. 15. Finally, it should be stated that nucleate boiling was absent in all experiments with the COP evaporator (with the possible exception of the eruptive boiling process described above) which were performed for wall temperatures of up to 93 °C.

3.3.2. Silicon evaporator

A part of the motivation for studying evaporation in the silicon microchannels depicted in Section 2 is their rough surface which potentially provides a large number of nucleation sites. In fact for a wall over-temperature (wall temperature − saturation temperature) of about 11 K bubble nucleation was observed in the silicon channels, whereas no bubbles were formed in the COP channels, with the possible exception of eruptive evaporation. This supports the hypothesis that the rough channel surfaces support bubble nucleation.

Nevertheless also the silicon evaporator exhibits flow regimes where bubble nucleation is largely absent, the regimes with stationary menisci and parallel oscillations described in Section 3.1.2. The occurrence of stationary menisci at a nonzero pump rate can only be explained by continuous evaporation at the liquid front. Presumably capillary forces constantly drive a thin liquid film in upstream direction along the rough channel walls where it evaporates. Comparing the four different evaporation modes in the silicon evaporator, the mode with stationary menisci leads to the highest heat transfer coefficient of about 4700 W/(m^2 K), where the wetted channel area was chosen as reference surface. The study of heat transfer performance, however, is not the focus of the present article but the subject of future work.

Comparing a cycle in the parallel oscillation regime with a cycle with continuous acceleration of the meniscus in the COP evaporator, a difference becomes apparent: when the meniscus recedes in the silicon channels, no liquid film at the channel walls is visible. The fact that no film was detected could be due to its limited visibility on the rough channel surfaces. However, in the nucleate boiling regime elongated vapor slugs are created which are separated from the walls by a thin liquid film. This film is clearly discernible on the photographic images, so that the conclusion may be drawn that in the parallel oscillation regime a possible liquid film remaining at the walls when the meniscus recedes should be very thin.

The question arises on what may be the driving mechanisms for the oscillations in the silicon channels. Another notable difference to the flow regime in the COP evaporator is the fact that liquid was pumped at a constant rate, whereas the COP channels were filled by capillary forces. Also in the silicon evaporator the vapor stream causes a viscous pressure drop, but the additional pressure drop in the liquid due to the pumping action may be large enough to prevent pushing back of the meniscus.

In fact there is evidence that the parallel oscillations observed are essentially due to evaporation and not due to liquid being pushed back. This evidence comes from computing the average speed of the menisci in the filling mode. The average speed was computed by integrating the sections of the curves in Figs. 17–19 with positive velocity and dividing the result by the appropriate time spans. The result of this computation may be compared with the liquid speed obtained by equally distributing the applied mass flow over the microchannels. The comparison shows that the velocity of the menisci in the filling mode is about a factor of two higher than the average speed due to pumping. Naturally, the fluidic capacities of the syringe pump and the connecting tube allows for momentary deviations from the applied average flow rate. However, the capacities also tend to level out such deviations. For these reasons it suggests itself to assume an evaporation mode with minimum deviations from the flow velocity derived from the average flow rate. In accordance with the measured filling speed of the channel, the evaporation mode fulfilling this criterion would be: (A) during filling (positive velocities) evaporation is negligible and (B) the observed retraction of the menisci is mainly due to evaporation, backflow of liquid (negative velocities) is largely suppressed.

This interpretation is also compatible with the shape of the velocity trajectories. Whereas for the COP evaporator a continuous acceleration of the evaporating menisci was detectable, those parts of the trajectories for the silicon evaporator with negative velocities show an almost immediate transition to the negative peak velocity. This is especially discernible in the individual curves, since averaging over the five individual data sets tends to smear out the sudden jump to negative velocities. Such a sudden jump with no significant acceleration phase may be explained by a meniscus receding mainly by evaporation rather than

by an induced backflow. When the meniscus reaches cooler regions in the upstream parts of the channel, the evaporation rate decreases and the motion is reversed.

Finally, there is yet another piece of evidence for the hypothesis of evaporation-induced retraction of the menisci. In a scenario where evaporation only plays a negligible role for the motion of a liquid front, a receding meniscus tends to induce an increased meniscus speed (in the direction of the main flow) in at least one parallel channel. The reasons for this "anticorrelation" between different channels are again the predefined volume flow and the fluidic capacities which tend to level out momentary variations of the total flow rate. Such a behavior has been found by Hetsroni et al. [11] who observed that when the liquid front is pushed back in one channel, the other channels carry the excess flow. In the present work, however, the menisci move in phase and the motion in different channels is correlated rather than anticorrelated.

It should be emphasized that the arguments in the preceding paragraphs are attempts to understand the observed evaporation mechanisms on the basis of the existing data. Cleary there is a need for refinement and extension of the experiments as well as for the development of sufficiently general mathematical models of evaporation in microchannels. Only in that way it will be possible to understand the dynamics and the mechanisms at work in detail.

4. Summary and conclusions

Evaporation phenomena in COP and silicon microchannels of 50 and 30 μm diameter have been studied experimentally. In contrast to most other studies in this area, it has been found that bubble nucleation is largely suppressed. Rather than that, evaporation modes with periodically advancing and receding liquid fronts dominate. The experiments reported in this paper were limited to the study of flow patterns which already display a variety of interesting phenomena. Different classes of flow patterns, depending on the wall temperature and the flow rate applied, have been identified. In summary, the most important results of the paper are

1. Two dominant flow patterns have been identified in the COP evaporator: film evaporation with continuous acceleration of the meniscus and film evaporation with preceding eruption. In both evaporation modes the liquid–vapor menisci perform a periodic motion and leave behind a thin liquid film on the walls when receding from the channels. When an eruption occurs, the meniscus is shifted in an almost discontinuous manner. Such eruptions occur close to imperfections of the channel walls and most probably originate from explosive bubble nucleation events. The corresponding dynamics is extremely fast and could not be resolved even at a frame rate of 5000 fps.
2. Velocity trajectories of the receding menisci in the COP channels have been recorded. The trajectories show a characteristic accelerated motion which has been explained with pressure forces acting on the liquid front and the increasing area of the liquid film covering the channel walls. The initial phase of the motion may vary for different cycles, however, the reproducibility of the trajectories is good when this initial phase is ignored.
3. Four different classes of flow patterns have been found for the silicon channels, where also the collective behavior of the evaporation process has been analyzed. In the parallel oscillation mode the oscillations in different channels are synchronized and in phase. In contrast to the COP channels, a receding meniscus does not leave a visible liquid film behind. When the mass flow is increased, the oscillations in different channels start to become desynchronized. At even higher mass flows this mode goes over in a nucleate boiling regime where frequently bubbles are found in the channels. The same transition may be induced by lowering the wall temperature at fixed mass flow (cf. Fig. 14). The latter stands in contrast to the usual pool boiling modes where a reduction of the wall temperature leads to a decrease of bubble nucleation.
4. The velocity trajectories for the silicon channels in the parallel oscillation mode show a characteristic asymmetric sawtooth shape, with a relatively slow increase and a rapid decrease in velocity. The reproducibility of the trajectories between different channels and different cycles is good, however, no clear relationship between the oscillation frequencies and amplitudes on the one hand and the wall temperature and mass flow on the other hand could be identified.

Acknowledgements

We are grateful to T. Hang for his support in the IR thermography measurements and to T. Klotzbücher for microchannel fabrication by laser ablation.

References

[1] C.J.M. Lasance, R.E. Simons, Advances in high-performance cooling for electronics, Electron. Cooling 11 (2005) 22–39.
[2] G. Kolb, V. Hessel, Micro-structured reactors for gas-phase reactions, Chem. Eng. J. 98 (2004) 1–38.
[3] V. Hessel, H. Löwe, A. Müller, G. Kolb, Chemical Micro Process Engineering: Processing and Plants, Wiley-VCH, Weinheim, 2005, Chapter 2.
[4] M.K. Drost, C. Call, J. Cuta, R. Wegeng, Microchannel combustor/evaporator thermal processes, Microscale Thermophys. Eng. 1 (1997) 321–332.
[5] S.G. Kandlikar, Fundamental issues related to flow boiling in minichannels and micro-channels, Exp. Thermal Fluid Sci. 26 (2002) 389–407.
[6] S.G. Kandlikar, P. Balasubramanian, An extension of the flow boiling correlation to transition, laminar, and deep laminar flows in minichannels and micro-channels, Heat Transfer Eng. 25 (2004) 86–93.

[7] J.R. Thome, Boiling in microchannels: a review of experiment and theory, Int. J. Heat Fluid Flow 25 (2004) 128–139.
[8] L. Jiang, M. Wong, Y. Zohar, Forced convection boiling in a microchannel heat sink, J. Microelectromech. Syst. 10 (2001) 80–87.
[9] G. Hetsroni, A. Mosyak, Z. Segal, E. Pogrebnyak, Two-phase flow patterns in parallel micro-channels, Int. J. Multiphase Flow 29 (2003) 341–360.
[10] G. Hetsroni, D. Klein, A. Mosyak, Z. Segal, E. Pogrebnyak, Convective boiling in parallel microchannels, Microscale Thermophys. Eng. 8 (2004) 403–421.
[11] G. Hetsroni, A. Mosyak, E. Pogrebnyak, Z. Segal, Explosive boiling of water in parallel micro-channels, Int. J. Multiphase Flow 31 (2005) 371–392.
[12] A. Serizawa, Z. Feng, Z. Kawara, Two-phase flow in microchannels, Exper. Thermal Fluid Sci. 26 (2002) 703–714.
[13] M.E. Steinke, S.G. Kandlikar, An experimental investigation of flow boiling characteristics of water in parallel microchannels, ASME J. Heat Transfer 126 (2004) 518–526.
[14] J. Lee, I. Mudawar, Two-phase flow in high-heat-flux micro-channel heat sink for refrigeration cooling applications: Part II—heat transfer characteristics, Int. J. Heat Mass Transfer 48 (2005) 941–955.
[15] H.Y. Li, F.G. Tseng, C. Pan, Bubble dynamics in microchannels. Part II: two parallel microchannels, Int. J. Heat Mass Transfer 47 (2004) 5591–5601.
[16] A. Koşar, C.J. Kuo, Y. Peles, Boiling heat transfer in rectangular microchannels with reentrant cavities, Int. J. Heat Mass Transfer 48 (2005) 4867–4886.
[17] A. Koşar, C.J. Kuo, Y. Peles, Reduced pressure boiling heat transfer in rectangular microchannels with interconnected reentrant cavities, ASME J. Heat Transfer 127 (2005) 1106–1114.
[18] A. Koşar, C.J. Kuo, Y. Peles, Supression of boiling flow oscillations in parallel microchannels by inlet restrictors, ASME J. Heat Transfer 128 (2006) 251–260.
[19] W. Qu, I. Mudawar, Transport phenomena in two-phase microchannel heat sinks, J. Electron. Packaging 126 (2004) 213–224.
[20] S. Kandlikar, W.K. Kuan, D.A. Willistein, J. Borelli, Stabilization of flow boiling in microchannels using pressure drop elements and fabricated nucleation sites, ASME J. Heat Transfer 128 (2006) 389–396.
[21] D. Liu, P.S. Lee, S.V. Garimella, Prediction of the onset of nucleate boiling in microchannel flow, Int. J. Heat Mass Transfer 48 (2005) 5134–5149.
[22] X.F. Peng, H.Y. Hu, B.X. Wang, Boiling nucleation during liquid flow in microchannels, Int. J. Heat Mass Transfer 41 (1998) 101–106.
[23] J. Xu, Y. Gan, D. Zhang, X. Li, Microscale boiling heat transfer in a micro-timescale at high heat fluxes, J. Micromech. Microeng. 15 (2005) 362–376.
[24] H.Y. Wu, P. Cheng, Boiling instability in parallel silicon microchannels at different heat flux, Int. J. Heat Mass Transfer 47 (2004) 3631–3641.
[25] L. Zhang, E.N. Wang, K.E. Goodson, T.W. Kenny, Phase change phenomena in silicon microchannels, Int. J. Heat Mass Transfer 48 (2005) 1572–1582.
[26] K. Park, K.S. Lee, Flow and heat transfer characteristics of the evaporating extended meniscus in a micro-capillary channel, Int. J. Heat Mass Transfer 46 (2003) 4587–4594.
[27] W. Qu, I. Mudawar, Flow boiling heat transfer in two-phase microchannel heat sinks—II. Annular two-phase flow model, Int. J. Heat Mass Transfer 46 (2003) 2773–2784.
[28] J.R. Thome, V. Dupont, A.M. Jacobi, Heat transfer model for evaporation in microchannels. Part I: presentation of the model, Int. J. Heat Mass Transfer 47 (2004) 3375–3385.
[29] V. Dupont, J.R. Thome, A.M. Jacobi, Heat transfer model for evaporation in microchannels. Part II: comparison with the database, Int. J. Heat Mass Transfer 47 (2004) 3387–3401.
[30] A. Mukherjee, S.G. Kandlikar, Numerical simulation of growth of a vapor bubble during flow boiling of water in a microchannel, Microfluid. Nanofluid. 1 (2005) 137–145.
[31] J. Li, P. Cheng, Bubble cavitation in a microchannel, Int. J. Heat Mass Transfer 47 (2004) 2689–2698.
[32] A. Griebel, S. Rund, F. Schönfeld, W. Dörner, R. Konrad, S. Hardt, Integrated polymer chip for two-dimensional capillary gel electrophoresis, Lab. Chip 4 (2004) 18–23.
[33] D.R. Lide (Ed.), Handbook of Chemistry and Physics, 79th ed., CRC Press, Boca Raton, FL, 1998.
[34] T. Hibiki, M. Ishii, Active nucleation site density in boiling systems, Int. J. Heat Mass Transfer 46 (2003) 2587–2601.